FERMILAB-PUB-09-013-E

Measurement of the $t\bar{t}$ production cross section and top quark mass extraction using dilepton events in $p\bar{p}$ collisions

V.M. Abazov[36], B. Abbott[75], M. Abolins[65], B.S. Acharya[29], M. Adams[51], T. Adams[49], E. Aguilo[6], M. Ahsan[59], G.D. Alexeev[36], G. Alkhazov[40], A. Alton[64,a], G. Alverson[63], G.A. Alves[2], M. Anastasoaie[35], L.S. Ancu[35], T. Andeen[53], B. Andrieu[17], M.S. Anzelc[53], M. Aoki[50], Y. Arnoud[14], M. Arov[60], M. Arthaud[18], A. Askew[49,b], B. Åsman[41], A.C.S. Assis Jesus[3], O. Atramentov[49], C. Avila[8], J. BackusMayes[82], F. Badaud[13], L. Bagby[50], B. Baldin[50], D.V. Bandurin[59], P. Banerjee[29], S. Banerjee[29], E. Barberis[63], A.-F. Barfuss[15], P. Bargassa[80], P. Baringer[58], J. Barreto[2], J.F. Bartlett[50], U. Bassler[18], D. Bauer[43], S. Beale[6], A. Bean[58], M. Begalli[3], M. Begel[73], C. Belanger-Champagne[41], L. Bellantoni[50], A. Bellavance[50], J.A. Benitez[65], S.B. Beri[27], G. Bernardi[17], R. Bernhard[23], I. Bertram[42], M. Besançon[18], R. Beuselinck[43], V.A. Bezzubov[39], P.C. Bhat[50], V. Bhatnagar[27], G. Blazey[52], F. Blekman[43], S. Blessing[49], K. Bloom[67], A. Boehnlein[50], D. Boline[62], T.A. Bolton[59], E.E. Boos[38], G. Borissov[42], T. Bose[77], A. Brandt[78], R. Brock[65], G. Brooijmans[70], A. Bross[50], D. Brown[19], X.B. Bu[7], N.J. Buchanan[49], D. Buchholz[53], M. Buehler[81], V. Buescher[22], V. Bunichev[38], S. Burdin[42,c], T.H. Burnett[82], C.P. Buszello[43], P. Calfayan[25], B. Calpas[15], S. Calvet[16], J. Cammin[71], M.A. Carrasco-Lizarraga[33], E. Carrera[49], W. Carvalho[3], B.C.K. Casey[50], H. Castilla-Valdez[33], S. Chakrabarti[72], D. Chakraborty[52], K.M. Chan[55], A. Chandra[48], E. Cheu[45], S. Chevalier-Thery[18], D.K. Cho[62], S. Choi[32], B. Choudhary[28], L. Christofek[77], T. Christoudias[43], S. Cihangir[50], D. Claes[67], J. Clutter[58], M. Cooke[50], W.E. Cooper[50], M. Corcoran[80], F. Couderc[18], M.-C. Cousinou[15], S. Crépé-Renaudin[14], V. Cuplov[59], D. Cutts[77], M. Ćwiok[30], H. da Motta[2], A. Das[45], G. Davies[43], K. De[78], S.J. de Jong[35], E. De La Cruz-Burelo[33], C. De Oliveira Martins[3], K. DeVaughan[67], F. Déliot[18], M. Demarteau[50], R. Demina[71], D. Denisov[50], S.P. Denisov[39], S. Desai[50], H.T. Diehl[50], M. Diesburg[50], A. Dominguez[67], T. Dorland[82], A. Dubey[28], L.V. Dudko[38], L. Duflot[16], S.R. Dugad[29], D. Duggan[49], A. Duperrin[15], S. Dutt[27], J. Dyer[65], A. Dyshkant[52], M. Eads[67], D. Edmunds[65], J. Ellison[48], V.D. Elvira[50], Y. Enari[77], S. Eno[61], P. Ermolov[38,‡], M. Escalier[15], H. Evans[54], A. Evdokimov[73], V.N. Evdokimov[39], A.V. Ferapontov[59], T. Ferbel[61,71], F. Fiedler[24], F. Filthaut[35], W. Fisher[50], H.E. Fisk[50], M. Fortner[52], H. Fox[42], S. Fu[50], S. Fuess[50], T. Gadfort[70], C.F. Galea[35], C. Garcia[71], A. Garcia-Bellido[71], V. Gavrilov[37], P. Gay[13], W. Geist[19], W. Geng[15,65], C.E. Gerber[51], Y. Gershtein[49,b], D. Gillberg[6], G. Ginther[71], B. Gómez[8], A. Goussiou[82], P.D. Grannis[72], H. Greenlee[50], Z.D. Greenwood[60], E.M. Gregores[4], G. Grenier[20], Ph. Gris[13], J.-F. Grivaz[16], A. Grohsjean[25], S. Grünendahl[50], M.W. Grünewald[30], F. Guo[72], J. Guo[72], G. Gutierrez[50], P. Gutierrez[75], A. Haas[70], N.J. Hadley[61], P. Haefner[25], S. Hagopian[49], J. Haley[68], I. Hall[65], R.E. Hall[47], L. Han[7], K. Harder[44], A. Harel[71], J.M. Hauptman[57], J. Hays[43], T. Hebbeker[21], D. Hedin[52], J.G. Hegeman[34], A.P. Heinson[48], U. Heintz[62], C. Hensel[22,d], K. Herner[72], G. Hesketh[63], M.D. Hildreth[55], R. Hirosky[81], T. Hoang[49], J.D. Hobbs[72], B. Hoeneisen[12], M. Hohlfeld[22], S. Hossain[75], P. Houben[34], Y. Hu[72], Z. Hubacek[10], N. Huske[17], V. Hynek[9], I. Iashvili[69], R. Illingworth[50], A.S. Ito[50], S. Jabeen[62], M. Jaffré[16], S. Jain[75], K. Jakobs[23], C. Jarvis[61], R. Jesik[43], K. Johns[45], C. Johnson[70], M. Johnson[50], D. Johnston[67], A. Jonckheere[50], P. Jonsson[43], A. Juste[50], E. Kajfasz[15], D. Karmanov[38], P.A. Kasper[50], I. Katsanos[70], V. Kaushik[78], R. Kehoe[79], S. Kermiche[15], N. Khalatyan[50], A. Khanov[76], A. Kharchilava[69], Y.N. Kharzheev[36], D. Khatidze[70], T.J. Kim[31], M.H. Kirby[53], M. Kirsch[21], B. Klima[50], J.M. Kohli[27], J.-P. Konrath[23], A.V. Kozelov[39], J. Kraus[65], T. Kuhl[24], A. Kumar[69], A. Kupco[11], T. Kurča[20], V.A. Kuzmin[38], J. Kvita[9], F. Lacroix[13], D. Lam[55], S. Lammers[70], G. Landsberg[77], P. Lebrun[20], W.M. Lee[50], A. Leflat[38], J. Lellouch[17], J. Li[78,‡], L. Li[48], Q.Z. Li[50], S.M. Lietti[5], J.K. Lim[31], J.G.R. Lima[52], D. Lincoln[50], J. Linnemann[65], V.V. Lipaev[39], R. Lipton[50], Y. Liu[7], Z. Liu[6], A. Lobodenko[40], M. Lokajicek[11], P. Love[42], H.J. Lubatti[82], R. Luna-Garcia[33,e], A.L. Lyon[50], A.K.A. Maciel[2], D. Mackin[80], R.J. Madaras[46], P. Mättig[26], A. Magerkurth[64], P.K. Mal[82], H.B. Malbouisson[3], S. Malik[67], V.L. Malyshev[36], Y. Maravin[59], B. Martin[14], R. McCarthy[72], M.M. Meijer[35], A. Melnitchouk[66], L. Mendoza[8], P.G. Mercadante[5], M. Merkin[38], K.W. Merritt[50], A. Meyer[21], J. Meyer[22,d], J. Mitrevski[70], R.K. Mommsen[44], N.K. Mondal[29], R.W. Moore[6], T. Moulik[58], G.S. Muanza[15], M. Mulhearn[70], O. Mundal[22], L. Mundim[3], E. Nagy[15], M. Naimuddin[50], M. Narain[77], H.A. Neal[64], J.P. Negret[8], P. Neustroev[40], H. Nilsen[23], H. Nogima[3], S.F. Novaes[5], T. Nunnemann[25], D.C. O'Neil[6], G. Obrant[40], C. Ochando[16], D. Onoprienko[59], N. Oshima[50], N. Osman[43], J. Osta[55], R. Otec[10], G.J. Otero y Garzón[1], M. Owen[44], M. Padilla[48], P. Padley[80], M. Pangilinan[77], N. Parashar[56], S.-J. Park[22,d], S.K. Park[31], J. Parsons[70], R. Partridge[77], N. Parua[54], A. Patwa[73], G. Pawloski[80], B. Penning[23], M. Perfilov[38], K. Peters[44], Y. Peters[26], P. Pétroff[16], M. Petteni[43], R. Piegaia[1], J. Piper[65], M.-A. Pleier[22], P.L.M. Podesta-Lerma[33,f], V.M. Podstavkov[50], Y. Pogorelov[55], M.-E. Pol[2], P. Polozov[37], B.G. Pope[65],

A.V. Popov[39], C. Potter[6], W.L. Prado da Silva[3], H.B. Prosper[49], S. Protopopescu[73], J. Qian[64], A. Quadt[22,d], B. Quinn[66], A. Rakitine[42], M.S. Rangel[2], K. Ranjan[28], P.N. Ratoff[42], P. Renkel[79], P. Rich[44], M. Rijssenbeek[72], I. Ripp-Baudot[19], F. Rizatdinova[76], S. Robinson[43], R.F. Rodrigues[3], M. Rominsky[75], C. Royon[18], P. Rubinov[50], R. Ruchti[55], G. Safronov[37], G. Sajot[14], A. Sánchez-Hernández[33], M.P. Sanders[17], B. Sanghi[50], G. Savage[50], L. Sawyer[60], T. Scanlon[43], D. Schaile[25], R.D. Schamberger[72], Y. Scheglov[40], H. Schellman[53], T. Schliephake[26], S. Schlobohm[82], C. Schwanenberger[44], R. Schwienhorst[65], J. Sekaric[49], H. Severini[75], E. Shabalina[51], M. Shamim[59], V. Shary[18], A.A. Shchukin[39], R.K. Shivpuri[28], V. Siccardi[19], V. Simak[10], V. Sirotenko[50], P. Skubic[75], P. Slattery[71], D. Smirnov[55], G.R. Snow[67], J. Snow[74], S. Snyder[73], S. Söldner-Rembold[44], L. Sonnenschein[17], A. Sopczak[42], M. Sosebee[78], K. Soustruznik[9], B. Spurlock[78], J. Stark[14], V. Stolin[37], D.A. Stoyanova[39], J. Strandberg[64], S. Strandberg[41], M.A. Strang[69], E. Strauss[72], M. Strauss[75], R. Ströhmer[25], D. Strom[53], L. Stutte[50], S. Sumowidagdo[49], P. Svoisky[35], A. Sznajder[3], A. Tanasijczuk[1], W. Taylor[6], B. Tiller[25], F. Tissandier[13], M. Titov[18], V.V. Tokmenin[36], I. Torchiani[23], D. Tsybychev[72], B. Tuchming[18], C. Tully[68], P.M. Tuts[70], R. Unalan[65], L. Uvarov[40], S. Uvarov[40], S. Uzunyan[52], B. Vachon[6], P.J. van den Berg[34], R. Van Kooten[54], W.M. van Leeuwen[34], N. Varelas[51], E.W. Varnes[45], I.A. Vasilyev[39], P. Verdier[20], L.S. Vertogradov[36], M. Verzocchi[50], D. Vilanova[18], F. Villeneuve-Seguier[43], P. Vint[43], P. Vokac[10], M. Voutilainen[67,g], R. Wagner[68], H.D. Wahl[49], M.H.L.S. Wang[50], J. Warchol[55], G. Watts[82], M. Wayne[55], G. Weber[24], M. Weber[50,h], L. Welty-Rieger[54], A. Wenger[23,i], N. Wermes[22], M. Wetstein[61], A. White[78], D. Wicke[26], M.R.J. Williams[42], G.W. Wilson[58], S.J. Wimpenny[48], M. Wobisch[60], D.R. Wood[63], T.R. Wyatt[44], Y. Xie[77], C. Xu[64], S. Yacoob[53], R. Yamada[50], W.-C. Yang[44], T. Yasuda[50], Y.A. Yatsunenko[36], Z. Ye[50], H. Yin[7], K. Yip[73], H.D. Yoo[77], S.W. Youn[53], J. Yu[78], C. Zeitnitz[26], S. Zelitch[81], T. Zhao[82], B. Zhou[64], J. Zhu[72], M. Zielinski[71], D. Zieminska[54], L. Zivkovic[70], V. Zutshi[52], and E.G. Zverev[38]

(The DØ Collaboration)

[1] *Universidad de Buenos Aires, Buenos Aires, Argentina*
[2] *LAFEX, Centro Brasileiro de Pesquisas Físicas, Rio de Janeiro, Brazil*
[3] *Universidade do Estado do Rio de Janeiro, Rio de Janeiro, Brazil*
[4] *Universidade Federal do ABC, Santo André, Brazil*
[5] *Instituto de Física Teórica, Universidade Estadual Paulista, São Paulo, Brazil*
[6] *University of Alberta, Edmonton, Alberta, Canada, Simon Fraser University, Burnaby, British Columbia, Canada, York University, Toronto, Ontario, Canada, and McGill University, Montreal, Quebec, Canada*
[7] *University of Science and Technology of China, Hefei, People's Republic of China*
[8] *Universidad de los Andes, Bogotá, Colombia*
[9] *Center for Particle Physics, Charles University, Prague, Czech Republic*
[10] *Czech Technical University, Prague, Czech Republic*
[11] *Center for Particle Physics, Institute of Physics, Academy of Sciences of the Czech Republic, Prague, Czech Republic*
[12] *Universidad San Francisco de Quito, Quito, Ecuador*
[13] *LPC, Université Blaise Pascal, CNRS/IN2P3, Clermont, France*
[14] *LPSC, Université Joseph Fourier Grenoble 1, CNRS/IN2P3, Institut National Polytechnique de Grenoble, Grenoble, France*
[15] *CPPM, Aix-Marseille Université, CNRS/IN2P3, Marseille, France*
[16] *LAL, Université Paris-Sud, IN2P3/CNRS, Orsay, France*
[17] *LPNHE, IN2P3/CNRS, Universités Paris VI and VII, Paris, France*
[18] *CEA, Irfu, SPP, Saclay, France*
[19] *IPHC, Université Louis Pasteur, CNRS/IN2P3, Strasbourg, France*
[20] *IPNL, Université Lyon 1, CNRS/IN2P3, Villeurbanne, France and Université de Lyon, Lyon, France*
[21] *III. Physikalisches Institut A, RWTH Aachen University, Aachen, Germany*
[22] *Physikalisches Institut, Universität Bonn, Bonn, Germany*
[23] *Physikalisches Institut, Universität Freiburg, Freiburg, Germany*
[24] *Institut für Physik, Universität Mainz, Mainz, Germany*
[25] *Ludwig-Maximilians-Universität München, München, Germany*
[26] *Fachbereich Physik, University of Wuppertal, Wuppertal, Germany*
[27] *Panjab University, Chandigarh, India*
[28] *Delhi University, Delhi, India*
[29] *Tata Institute of Fundamental Research, Mumbai, India*
[30] *University College Dublin, Dublin, Ireland*
[31] *Korea Detector Laboratory, Korea University, Seoul, Korea*
[32] *SungKyunKwan University, Suwon, Korea*
[33] *CINVESTAV, Mexico City, Mexico*

[34] FOM-Institute NIKHEF and University of Amsterdam/NIKHEF, Amsterdam, The Netherlands
[35] Radboud University Nijmegen/NIKHEF, Nijmegen, The Netherlands
[36] Joint Institute for Nuclear Research, Dubna, Russia
[37] Institute for Theoretical and Experimental Physics, Moscow, Russia
[38] Moscow State University, Moscow, Russia
[39] Institute for High Energy Physics, Protvino, Russia
[40] Petersburg Nuclear Physics Institute, St. Petersburg, Russia
[41] Lund University, Lund, Sweden, Royal Institute of Technology and Stockholm University, Stockholm, Sweden, and Uppsala University, Uppsala, Sweden
[42] Lancaster University, Lancaster, United Kingdom
[43] Imperial College, London, United Kingdom
[44] University of Manchester, Manchester, United Kingdom
[45] University of Arizona, Tucson, Arizona 85721, USA
[46] Lawrence Berkeley National Laboratory and University of California, Berkeley, California 94720, USA
[47] California State University, Fresno, California 93740, USA
[48] University of California, Riverside, California 92521, USA
[49] Florida State University, Tallahassee, Florida 32306, USA
[50] Fermi National Accelerator Laboratory, Batavia, Illinois 60510, USA
[51] University of Illinois at Chicago, Chicago, Illinois 60607, USA
[52] Northern Illinois University, DeKalb, Illinois 60115, USA
[53] Northwestern University, Evanston, Illinois 60208, USA
[54] Indiana University, Bloomington, Indiana 47405, USA
[55] University of Notre Dame, Notre Dame, Indiana 46556, USA
[56] Purdue University Calumet, Hammond, Indiana 46323, USA
[57] Iowa State University, Ames, Iowa 50011, USA
[58] University of Kansas, Lawrence, Kansas 66045, USA
[59] Kansas State University, Manhattan, Kansas 66506, USA
[60] Louisiana Tech University, Ruston, Louisiana 71272, USA
[61] University of Maryland, College Park, Maryland 20742, USA
[62] Boston University, Boston, Massachusetts 02215, USA
[63] Northeastern University, Boston, Massachusetts 02115, USA
[64] University of Michigan, Ann Arbor, Michigan 48109, USA
[65] Michigan State University, East Lansing, Michigan 48824, USA
[66] University of Mississippi, University, Mississippi 38677, USA
[67] University of Nebraska, Lincoln, Nebraska 68588, USA
[68] Princeton University, Princeton, New Jersey 08544, USA
[69] State University of New York, Buffalo, New York 14260, USA
[70] Columbia University, New York, New York 10027, USA
[71] University of Rochester, Rochester, New York 14627, USA
[72] State University of New York, Stony Brook, New York 11794, USA
[73] Brookhaven National Laboratory, Upton, New York 11973, USA
[74] Langston University, Langston, Oklahoma 73050, USA
[75] University of Oklahoma, Norman, Oklahoma 73019, USA
[76] Oklahoma State University, Stillwater, Oklahoma 74078, USA
[77] Brown University, Providence, Rhode Island 02912, USA
[78] University of Texas, Arlington, Texas 76019, USA
[79] Southern Methodist University, Dallas, Texas 75275, USA
[80] Rice University, Houston, Texas 77005, USA
[81] University of Virginia, Charlottesville, Virginia 22901, USA and
[82] University of Washington, Seattle, Washington 98195, USA

(Dated: January 14, 2009)

We present a measurement of the top quark pair production cross section in $p\bar{p}$ collisions at $\sqrt{s} =$ 1.96 TeV using approximately 1 fb^{-1} of data collected with the D0 detector. We consider decay channels containing two high p_T charged leptons where one lepton is identified as an electron or a muon while the other lepton can be an electron, a muon or a hadronically decaying τ lepton. For a mass of the top quark of 170 GeV, the measured cross section is $7.5^{+1.0}_{-1.0}$ (stat) $^{+0.7}_{-0.6}$ (syst) $^{+0.6}_{-0.5}$ (lumi) pb. Using $\ell\tau$ events only, we measure: $\sigma_{t\bar{t}} \times B(t\bar{t} \to \ell\tau b\bar{b}) = 0.13^{+0.09}_{-0.08}(\text{stat})^{+0.06}_{-0.06}(\text{syst})^{+0.02}_{-0.02}(\text{lumi})$ pb. Comparing the measured cross section as a function of the mass of the top quark with a partial next-to-next-to leading order Quantum Chromodynamics theoretical prediction, we extract a mass of the top quark of $171.5^{+9.9}_{-8.8}$ GeV, in agreement with direct measurements.

PACS numbers: 14.65.Ha, 13.85.Lg, 13.85.Qk, 14.60Fg, 12.15.Ff

The top quark, first observed at Fermilab in 1995 [1, 2], is the heaviest known elementary particle. In many extensions of the standard model (SM) new physics is predicted in connection with top quarks. In the SM, top quarks are predicted to decay into a W boson and a b quark with a branching fraction of nearly 100% [3]. For approximately 10% of all top-antitop quark ($t\bar{t}$) events, both W bosons decay leptonically and generate final states containing two leptons [3]. In addition, these final states are characterized by the presence of two high energy jets resulting from hadronization of the two b quarks and large imbalance in transverse momentum ($\not\!\!E_T$) due to several undetected neutrinos from the W boson decays.

New physics in the production or decay of top quark may lead to significant deviations in the measured $t\bar{t}$ cross section ($\sigma_{t\bar{t}}$) from the SM prediction. Since new physics could have a different impact on different final states, it is important to measure $\sigma_{t\bar{t}}$ precisely in all possible decay channels. If, for instance, the top quark decayed into a charged Higgs boson ($H^{\pm}$) as is suggested in supersymmetric (SUSY) extensions of the SM [4], and the $H^{\pm}$ decayed predominantly into a τ lepton and a τ neutrino as it is the case in certain regions of the SUSY parameter space, the $t\bar{t} \to \ell\tau b\bar{b}$ final state (where ℓ is an electron or a muon) would be enhanced relative to its SM expectation. Owing to the significant dependence of the $t\bar{t}$ cross section on the mass of the top quark (m_t), a precise cross section measurement allows the extraction of the mass of the top quark in a way complementary to direct reconstruction methods and hence to perform a valuable consistency check. A precise measurement of the mass of the top quark is important since together with that of the W boson, it allows one to place indirect constraints on the mass of the SM Higgs boson.

In this Letter, we present a measurement of $\sigma_{t\bar{t}}$ using approximatively 1 fb^{-1} of data from Run II of the Fermilab Tevatron $p\bar{p}$ collider operated at $\sqrt{s} = 1.96$ TeV, and collected with the D0 detector. We consider dilepton final states with two identified electrons or muons from the W boson leptonic decays, i.e., ee, $e\mu$ and $\mu\mu$, and final states with a τ lepton that decays into hadrons+ν_τ from the decay of one W boson and an accompanying electron or muon from the other W boson, i.e., $e\tau$ and $\mu\tau$. Throughout the text, these final states will be referred to as $\ell\ell$ and $\ell\tau$ channels, respectively. Dilepton channels also have contributions from events where both τ leptons decay into electrons or muons. Previous measurements of $\sigma_{t\bar{t}}$ in the dilepton channel were reported in [5, 6]. We update the D0 measurement [5] using more integrated luminosity and include the $\ell\tau$ final states in the result. We also present a measurement of $\sigma_{t\bar{t}} \times B(t\bar{t} \to \ell\tau b\bar{b})$. In addition, we explore the dependence of $\sigma_{t\bar{t}}$ on the mass of the top quark, and through a comparison with higher order Quantum Chromodynamics (QCD) calculations computed in the pole mass scheme, we extract a value for the mass of the top quark.

The D0 detector has a central tracking system, consisting of a silicon microstrip tracker (SMT) and a central fiber tracker, both located within a 2 T superconducting solenoidal magnet [7]. A liquid argon and uranium calorimeter has a central section covering pseudorapidities $|\eta|$ up to ≈ 1.1 [8], and two end calorimeters (EC) that extend coverage to $|\eta| \approx 4.2$, with all three calorimeters housed in separate cryostats [9]. An outer muon system, covering $|\eta| < 2$, consists of a layer of tracking detectors and scintillation trigger counters in front of 1.8 T iron toroids, followed by two similar layers after the toroids [10]. The luminosity is measured using plastic scintillator arrays placed in front of the EC cryostats. The trigger and data acquisition systems are designed to accommodate the high luminosities of Run II. The dilepton triggers used in the $\ell\ell$ channels are described in Ref. [5]. The $\ell\tau$ channel uses triggers requiring one lepton and one jet. The typical trigger efficiency for signal events varies from 78% to 98% depending on the channel.

Electrons are identified as clusters of energy deposits in calorimeter cells satisfying the following requirements: (i) the fraction of energy deposited in the electromagnetic section of the calorimeter is at least 90% of the total cluster energy, (ii) the energy is concentrated in a narrow cone, and isolated from other energy deposits, (iii) the shape of the shower is compatible with that of an electron, and (iv) a track extrapolated from the tracking system points to the cluster. To further reduce backgrounds (see below for background description) we use a likelihood discriminant that selects prompt isolated electrons, based on tracking and calorimetric information. Both central ($|\eta| < 1.1$) and forward ($1.5 < |\eta| < 2.5$) electron candidates are accepted. Electrons that fulfill all the above criteria are referred to as "tight" electrons.

Muon trajectories are reconstructed using hits in three layers of the outer muon system along with matching tracks in the inner tracker. The energy deposited within an annulus $0.1 < \sqrt{(\Delta\eta)^2 + (\Delta\phi)^2} < 0.4$ around the muon direction (where ϕ is the azimuthal angle) must be less than 15% of the muon p_T, for all channels except $\mu\mu$, while for the $\mu\mu$ final state, the selected muons must not lie within the cone of any reconstructed jet. To reduce background further, the sum of the track momenta in a cone around the muon track has to be smaller than 15% of the muon p_T. Moreover, the fraction of prompt muons is increased by requiring that the distance of closest approach of the muon track to the primary vertex is small.

A hadronically decaying τ lepton is characterized by a narrow jet of low track multiplicity. The τ lepton reconstruction is seeded either by a calorimetric energy cluster or by a track. Three types of τ decays are defined as (i) τ-type 1 ($\pi^{\pm}$-like), consisting of a single track, with energy deposition in the hadronic calorimeter, (ii) τ-type 2 ($\rho^{\pm}$-like), a single track, with an energy deposit in both the hadronic and the electromagnetic calorimeters and (iii) τ-type 3, having two or three tracks, forming an invariant mass < 1.1 or < 1.7 GeV, respectively. The total sum of the particle charges for τ-type 3 is required to be ± 1 or ± 2. A set of neural networks (NN_τ), one for

each τ-type, has been developed based on discriminating variables discussed in Ref. [11]. These variables exploit differences between hadronically decaying τ leptons and jets resulting from the fragmentation of quarks and gluons, in particular the longitudinal and transverse shower shapes as well as isolation in the calorimeter and in the tracker.

Jets are reconstructed using a fixed cone algorithm with radius $\mathcal{R} = 0.5$ [12]. A jet energy scale calibration obtained from transverse momentum balance in γ+jet events is applied to all jets. $\not\!\!E_T$ is defined as equal in magnitude and opposite in direction to the vector sum of all significant transverse energies in calorimeter cells. It is further corrected by the transverse momentum of all reconstructed muons, as well as by the energy calibration corrections applied to the transverse momenta of electrons, τ leptons and jets. A more detailed description of object reconstruction can be found in Ref. [5].

Jets from b quarks are identified using a neural network b jet tagging algorithm [13]. It combines several variables that characterize the presence and properties of the secondary vertices and the tracks of high impact parameter within jets. We obtain a 54% average tagging efficiency in data for b jets [13], which corresponds to a 1% mistagging of jets from light quark flavors (u, d or s quarks) as b jets.

In the $\ell\ell$ channels, the main source of background is the production of electroweak bosons that decay to charged leptons. It arises from $Z/\gamma^* \to \ell^+\ell^-$ and $Z/\gamma^* \to \tau^+\tau^-$, followed by $\tau \to \ell^\pm\nu_\ell\nu_\tau$ with $\ell^\pm = e^\pm$ or $\mu^\pm$, along with diboson production (WW, WZ and ZZ), when the boson decays lead to at least two charged leptons in the final state. In the $\ell\tau$ channel, the dominant background emerges from jets mimicking electrons and τ leptons, muons from semileptonic b quark decay or pion or kaon decay, and large misreconstructed $\not\!\!E_T$, mainly in W+jets and multijet production.

The event selection for each channel is optimized through a minimization of the expected statistical uncertainty on the cross section using Monte Carlo (MC). Signal $t\bar{t}$ events are required to have one isolated electron or muon for the $\ell\tau$ channel or two isolated oppositely charged leptons for the $\ell\ell$ channels. At least one jet is required to have $p_T > 30$ GeV. All channels, except for $e\mu$, which has the best signal over background ratio, require another jet with $p_T > 20$ GeV. Jets are accepted in the region $|\eta| < 2.5$. Leptons are required to have $p_T > 15$ GeV in the $\ell\ell$ channels. A muon in the $\mu\tau$ channel is required to have $p_T > 20$ GeV and an electron in the $e\tau$ channel $p_T > 15$ GeV. Tau leptons are required to have $E_T > 10$, 5, or 10 GeV for $\tau-$type 1, 2 or 3 respectively. Muons are accepted in the region $|\eta| < 2.0$, while electrons must be within $|\eta| < 1.1$ or $1.5 < |\eta| < 2.5$. In the $\ell\tau$ channels, events containing any additional isolated electron or muon are rejected in order to reduce $Z/\gamma^* \to \ell^+\ell^-$ background and to ensure that the $\ell\tau$ channels have no overlap with the $\ell\ell$ channels. Furthermore, if more than one τ lepton is found in an event, only the one with highest τ probability (highest NN_τ [11] value) is kept for further analysis.

The selection on $\not\!\!E_T$ is crucial for reducing the otherwise large background from $Z/\gamma^* \to \ell^+\ell^-$. This background is particularly important in the ee, $\mu\mu$ and $\ell\tau$ channels. Due to different resolutions in electron energies and muon momenta, optimization of selections leads to different criteria for the four channels. In the ee channel, events with dielectron invariant mass of $M_{ee} < 15$ GeV or $84 < M_{ee} < 100$ GeV are rejected. For $M_{ee} > 100$ GeV ($15 < M_{ee} < 84$ GeV), they are required to have $\not\!\!E_T > 35$ GeV ($\not\!\!E_T > 45$ GeV). The final selection in the $e\mu$ channel requires the scalar sum of the most energetic (leading) lepton p_T and the p_T of the single jet (two most energetic jets) to be $H_T > 105$ GeV ($H_T > 115$ GeV). This requirement rejects the largest backgrounds in this final state, which arise from $Z/\gamma^* \to \tau^+\tau^-$ and diboson production. In the $\mu\mu$ channel, events are required to have $\not\!\!E_T > 40$ GeV. The dimuon invariant mass $M_{\mu\mu}$ must be larger than 30 GeV. To reduce $Z/\gamma^* \to \mu^+\mu^-$ background, we define a likelihood ratio variable based on the per-event $\not\!\!E_T$ probability distribution, calculated from the expected resolution on $\not\!\!E_T$ and the energies of electrons, muons and jets. This $\not\!\!E_T$ likelihood ratio variable is required to be larger than 5. For $\ell\tau$ channels, events are required to have $15 < \not\!\!E_T < 200$ GeV. To reduce the multijet background, a two dimensional selection is applied in the $(\Delta\phi(\not\!\!E_T, \ell), \not\!\!E_T)$ plane where $\Delta\phi(\not\!\!E_T, \ell)$ is the difference between the azimuthal angle of the $\not\!\!E_T$ direction and of the lepton: $\Delta\phi(\not\!\!E_T, e) > 2.2 - 0.045 \times \not\!\!E_T(\text{GeV})$ in the $e\tau$ channel and $\Delta\phi(\not\!\!E_T, \mu) > 2.1 - 0.035 \times \not\!\!E_T(\text{GeV})$ in the $\mu\tau$ channel. Furthermore, in the $e\tau$ channel, events with electrons and $\not\!\!E_T$ collinear are rejected by requiring $\cos(\Delta\phi(\not\!\!E_T, e)) < 0.9$. In the $\mu\tau$ channel, events with a second non-isolated muon are rejected if the invariant mass of the two muons lies in the mass range $70 < M_{\mu\mu} < 100$ GeV. The final selection in the $\ell\tau$ channels requires at least one b-tagged jet.

The acceptance and efficiency for $t\bar{t}$ signal are derived from a combination of MC simulation and data. Top quark pair production is simulated using the ALPGEN [14] matrix element generator, assuming m_t=170 GeV. These events are processed through PYTHIA [15] to simulate fragmentation, hadronization and particle decays and then passed through a GEANT3 [16] based simulation of the D0 detector. Data events from random $p\bar{p}$ crossings are superimposed on MC generated events to reproduce detector noise and luminosity dependent effects in data. The same reconstruction process is applied to both data and MC events to determine the selection efficiencies. Lepton trigger and identification efficiencies, as well as lepton momentum resolution, are derived from $Z/\gamma^* \to \ell^+\ell^-$ data by identifying one tight charged lepton as tag and using the other charged lepton as a probe. The efficiencies are studied in different detector regions and as a function of the number of jets. The lepton and jet reconstruction efficiencies, as well as the lepton, jet

energy and $\not\!\!E_T$ resolutions in the MC are adjusted to the values measured in data.

Background contributions are also determined from a combination of MC simulation and data. The selection efficiencies for the Z/γ^* and W+jets backgrounds are estimated using MC samples generated by ALPGEN interfaced with PYTHIA while for diboson production they are estimated using PYTHIA. The Z/γ^* and diboson processes are generated at leading order (LO) and are normalized to the next-to-next-to-leading order (NNLO) inclusive cross section and to the next-to-leading order (NLO) inclusive cross sections, respectively [17, 18]. As the p_T distribution of the Z boson is not well described in the ALPGEN simulation, the p_T spectrum was reweighted to reproduce that in $Z \to e^+e^-$ data in the different jet multiplicities.

In the $\ell\tau$ channel, the simulated inclusive background from $W+ \geq 2$ jet events is normalized by fitting the transverse mass distribution [19] of the isolated lepton and $\not\!\!E_T$ to data. We estimate the multijet background from data using events having an electron or muon and a τ lepton of the same-charge (after subtracting contributions from W and same-charge $t\bar{t}$ MC events). The $t\bar{t}$ contributions to the same-charge sample result either from a jet reconstructed as a τ lepton or from a misidentification of the charge of the τ lepton. Contributions from Z/γ^* and diboson events to the same-charge sample are negligible.

In the $\ell\ell$ channel, the instrumental background is also determined from data. False electrons can arise from jets comprised of an energetic π^0 or η, and an overlapping track from $\gamma \to e^+e^-$ conversion. In the ee and $e\mu$ channels, the background from false electrons is fitted to the distribution of the electron likelihood discriminant in the data as done in Ref. [5]. The shape of the electron likelihood is determined for true electrons in a $Z/\gamma^* \to e^+e^-$ data sample. The shape of the electron likelihood for background electrons is then determined using a data sample with low $\not\!\!E_T$ dominated by false electrons. An isolated muon can be mimicked by a muon in a jet when the jet is not reconstructed. We measure the fraction f_μ of muons that appear isolated in a sample enriched in semileptonic decays of heavy flavor quarks and in pions or kaons semileptonic in-flight decays. In this sample, one of the muons is required not to be isolated while the second serves as a probe. In the $\mu\mu$ channel the number of events with a false isolated muon that contribute to the final sample is evaluated as in Ref. [5]. In the $e\mu$ channel, the contribution from events with a true electron and a false isolated muon is given by the number of events in a sample without a muon isolation requirement (where the electron and the muon have the same charge) multiplied by the rate f_μ introduced above. Although the $Z/\gamma^* \to \ell^+\ell^-$ processes do not lead to high p_T neutrinos, they can have large $\not\!\!E_T$ from mismeasurements. The $\not\!\!E_T$ spectra from $Z/\gamma^* \to \ell^+\ell^-$ data and the MC agree well, after jet, electron and muon resolutions are adjusted in the MC to match the resolutions observed in data.

In the $\ell\tau$ channel, instrumental background can arise from a candidate electron that does not satisfy electron selection criteria but can mimic the signatures of a type 2 τ lepton. To discriminate between the τ-type 2 leptons and electrons, we use another neural network ($NN_{\rm e}$) [11] along with NN_τ. The $NN_{\rm e}$ neural network relies on a subset of the input variables to NN_τ and on other variables based on the properties of the electromagnetic clusters and on the correlation between them and those of the leading track of the τ lepton. In addition, in the $e\tau$ channel, τ lepton candidates with track $\phi < 0.02$ radian from the nearest border of the calorimeter module are removed since they are more likely coming from misreconstructed electrons. A τ lepton can also be mimicked by a jet. The corresponding rate for such misidentification is determined through a correction factor from a comparison of W+jets MC samples to e+jets data, where the estimated contribution from multijet events as well as from $Z \to e^+e^-$, $Z \to \tau^+\tau^-$ and $t\bar{t}$ have been subtracted via MC. This correction factor is then applied to the W+jets and $t\bar{t} \to \ell$+jets samples.

The expected number of background and signal events and the number observed in data as well as the selection efficiencies and luminosities are summarized for all channels in Table I. Figure 1 shows the expected and observed distributions for several observables in the combined $\ell\ell$ and $\ell\tau$ channels. Figure 2 shows distributions in τ-types and E_T of the τ lepton in the $\ell\tau$ channels.

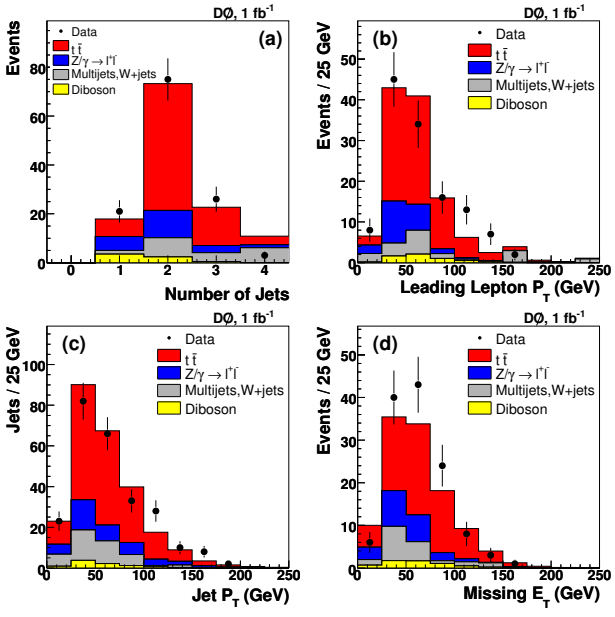

FIG. 1: Expected and observed distributions for the combined $\ell\ell$ and $\ell\tau$ channels for events with ≥ 1 jet ($e\mu$) or ≥ 2 jets (ee, $\mu\mu$, $\ell\tau$) following all selections for (a) the number of jets per event, (b) leading lepton p_T, (c) jet p_T, and (d) $\not\!\!E_T$. The $t\bar{t}$ contribution is normalized to the cross section measured in this analysis.

The systematic uncertainty on the measured $t\bar{t}$ pro-

TABLE I: Expected number of background and signal events, observed number of events in data, selection efficiencies and luminosities for all dilepton channels. Uncertainties include both statistical and systematic contributions (excluding luminosity uncertainty of 6.1% [20]). In the $\ell\tau$ channel, only hadronically decaying τ leptons are considered. The signal efficiency is quoted for m_t=170 GeV and the expected number of signal events for $\sigma_{t\bar{t}} = 7.9$ pb [21].

Channel	ee	$e\mu$ (1 jet)	$e\mu$ ($\geq$ 2 jets)	$\mu\mu$	$e\tau$	$\mu\tau$
Luminosity (pb^{-1})	1074	1070	1070	1009	1038	996
Z/γ^*	$2.4^{+0.6}_{-0.5}$	$5.5^{+0.7}_{-0.8}$	$5.4^{+0.9}_{-1.0}$	$5.6^{+1.0}_{-1.2}$	$0.6^{+0.1}_{-0.1}$	$1.2^{+0.3}_{-0.2}$
$WW/WZ/ZZ$	$0.5^{+0.1}_{-0.1}$	$3.1^{+0.7}_{-0.7}$	$1.4^{+0.4}_{-0.4}$	$0.6^{+0.1}_{-0.1}$	$0.2^{+0.0}_{-0.0}$	$0.2^{+0.0}_{-0.0}$
Multijet/W+jets	$0.6^{+0.4}_{-0.4}$	$0.9^{+0.3}_{-0.2}$	$2.6^{+0.6}_{-0.5}$	$0.2^{+0.2}_{-0.2}$	$3.6^{+1.8}_{-1.8}$	$8.8^{+2.8}_{-2.8}$
Total background	$3.4^{+0.7}_{-0.6}$	$9.5^{+1.0}_{-1.1}$	$9.4^{+1.2}_{-1.2}$	$6.4^{+1.9}_{-1.1}$	$4.4^{+1.8}_{-1.8}$	$10.2^{+2.9}_{-2.9}$
Signal efficiency (%)	$1.3^{+0.1}_{-0.1}$	$1.0^{+0.0}_{-0.0}$	$3.9^{+0.0}_{-0.0}$	$1.1^{+0.0}_{-0.0}$	$0.23^{+0.1}_{-0.1}$	$0.28^{+0.1}_{-0.1}$
Expected signal	$11.2^{+0.8}_{-0.8}$	$8.6^{+1.1}_{-1.1}$	$35.2^{+2.6}_{-2.7}$	$8.8^{+0.8}_{-0.8}$	$10.3^{+1.1}_{-1.1}$	$12.2^{+1.1}_{-1.1}$
Total expected	$14.6^{+1.0}_{-1.0}$	$18.0^{+1.4}_{-1.6}$	$44.6^{+3.4}_{-3.6}$	$15.1^{+1.5}_{-1.6}$	$14.7^{+2.0}_{-2.0}$	$22.3^{+3.1}_{-3.1}$
Data	17	21	39	12	16	20

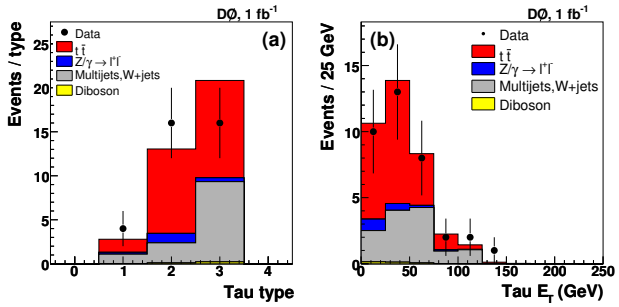

FIG. 2: Expected and observed distributions in the $\ell\tau$ channel for (a) the τ-type and (b) E_T of the τ lepton. The $t\bar{t}$ contribution is normalized to the cross section measured in the $\ell\tau$ channel. Only events with hadronically decaying τ leptons are considered.

duction cross section in the dilepton channel is obtained by varying the efficiencies and background contributions within their uncertainties, taking all correlations among the different channels and background contributions into account. The statistical uncertainties on MC and backgrounds are treated as uncorrelated among channels, while other sources of systematic uncertainty are treated as correlated. The dominant systematic uncertainties are summarized in Table II for individual channels and in Table III for the combination of channels.

The systematic uncertainties on trigger efficiencies ($\sim$2% of the cross section) are derived from data. Various sources of bias are investigated, and the resulting changes in trigger efficiencies are included as systematic uncertainties.

The systematic uncertainty for identifying τ lepton ($\sim$ 5.5% of the $\ell\tau$ cross section) arises dominantly from the uncertainty on the data to MC agreement and from the statistical uncertainty on the correction factor for jets mimicking τ leptons. The systematic uncertainty for the τ lepton energy scale ($\sim$ 6% of the $\ell\tau$ cross section) is estimated from the calorimeter's response to single pions [11].

The systematic uncertainties from the reconstruction and resolution of jets ($\sim$ 1%) are determined from the uncertainty on the data/MC correction factors. The uncertainty on the calibration of jet energy ($\sim$4%) is propagated to the predicted background and to the efficiency for $t\bar{t}$ signal.

The uncertainty on b tagging specific to the $\ell\tau$ channel ($\sim$4.5%) is evaluated by shifting the jet tagging probability within its uncertainty. The flavor dependent uncertainties are evaluated by changing the parametrization of the tagging probability for different types of jets (b, c and light jets).

The uncertainty on theoretical modeling of $t\bar{t}$ production ($\sim$5%) is estimated by comparing the acceptance of the two MC programs, PYTHIA and ALPGEN. The full difference in the final result is quoted as the systematic uncertainty. Half of the difference between unity and the ratio of the NLO diboson cross section to the LO diboson cross section (used to scale the diboson cross sections in PYTHIA) is taken as a systematic uncertainty for the diboson background. The systematic uncertainty on the normalization of the Z/γ^* background is estimated by propagating the uncertainty on the p_T reweighting function of the Z boson.

The systematic uncertainties on electron background in the $e\mu$ and ee channels are evaluated using the shape dependence of the electron likelihood discriminant on electron p_T and the detector occupancy (number of jets).

Other smaller sources of systematic uncertainties ($\sim$2.5%) arise from vertex identification, parton distribution functions and $\not\!\!E_T$ modeling. The luminosity uncertainty ($\sim$6%) [20] on the cross sections is evaluated taking into account both the uncertainty on the predicted number of signal and background events.

Cross sections for individual channels are extracted using a likelihood technique described in Ref. [5]. The results are presented in Table IV. All cross sections agree

TABLE II: Summary of the effects of individual systematic uncertainties on the measured cross section (in pb).

Source	ee	$e\mu$ (1 jet)	$e\mu$ ($\geq$ 2 jets)	$\mu\mu$	$e\tau$	$\mu\tau$
Trigger	+0.0 -0.0	+0.6 +0.0	+0.2 -0.0	+0.6 -0.4	+0.2 -0.1	+0.3 -0.2
Lepton identification	+0.4 -0.4	+0.5 -0.5	+0.2 -0.2	+0.5 -0.4	+0.3 -0.2	+0.2 -0.2
Tau identification	n/a	n/a	n/a	n/a	+0.6 -0.5	+0.4 -0.3
Tau energy scale	n/a	n/a	n/a	n/a	+0.5 -0.4	+0.4 -0.4
Jet identification	+0.1 -0.2	+0.4 -0.4	+0.1 -0.1	+0.2 -0.4	+0.1 -0.1	+0.1 -0.1
Jet energy scale	+0.6 -0.5	+0.8 -0.7	+0.5 -0.5	+0.6 -0.2	+0.2 -0.2	+0.3 -0.2
b jet identification	n/a	n/a	n/a	n/a	+0.4 -0.4	+0.3 -0.3
Signal modeling	+0.4 -0.4	+1.1 -1.0	+0.3 -0.3	+0.3 -0.3	+1.0 -0.8	+0.6 -0.5
Background estimation	+0.2 -0.1	+0.6 -0.5	+0.1 -0.1	+0.4 -0.3	+0.1 -0.1	+0.1 -0.1
False lepton background	+0.3 -0.3	+0.2 -0.3	+0.1 -0.1	+0.1 -0.1	+1.3 -1.3	+1.8 -1.8
Other	+0.4 -0.4	+0.7 -0.7	+0.2 -0.2	+0.7 -0.7	+0.3 -0.3	+0.2 -0.2
Total	+1.0 -0.9	+1.9 -1.6	+0.8 -0.7	+1.3 -1.1	+1.9 -1.8	+2.1 -2.0
Luminosity	+0.8 -0.7	+1.2 -1.1	+0.5 -0.5	+0.7 -0.6	+0.6 -0.5	+0.5 -0.4

TABLE III: Summary of the effects of individual systematic uncertainties on the combined cross section (in pb).

Source	dilepton ($\ell\ell$)	combined ($\ell\ell$ + $\ell\tau$)
Trigger	+0.2 -0.1	+0.2 -0.1
Lepton identification	+0.2 -0.2	+0.2 -0.2
Tau identification	n/a	+0.1 -0.1
Tau energy scale	n/a	+0.1 -0.1
Jet identification	+0.0 -0.1	+0.0 -0.0
Jet energy scale	+0.4 -0.4	+0.3 -0.3
b jet identification	n/a	+0.1 -0.1
Signal modeling	+0.3 -0.3	+0.4 -0.4
Background estimation	+0.2 -0.1	+0.1 -0.1
False lepton background	+0.1 -0.1	+0.3 -0.3
Other	+0.3 -0.3	+0.2 -0.2
Total	+0.7 -0.6	+0.7 -0.6
Luminosity	+0.7 -0.5	+0.6 -0.5

within their uncertainties. The combined result is obtained by minimizing the sum of negative log-likelihood functions from the five channels. All systematic uncertainties are incorporated in the fit as "nuisance parameters" [22] that can affect the central value of the cross section. The result from combining the ee, $e\mu$ and $\mu\mu$ ($\ell\ell$) channels is:

$$\sigma_{t\bar{t}} = 7.5^{+1.2}_{-1.1}\,(\text{stat})\,^{+0.7}_{-0.6}\,(\text{syst})\,^{+0.7}_{-0.5}\,(\text{lumi})\,\text{pb}$$

TABLE IV: The measured $t\bar{t}$ cross section at $\sqrt{s} = 1.96$ TeV for m_t=170 GeV. In the $\ell\tau$ channel, only hadronically decaying τ leptons are considered.

Channel	$\sigma_{t\bar{t}}$ (pb)
ee	$9.6^{+3.2}_{-2.7}\,(\text{stat})\,^{+1.0}_{-0.9}\,(\text{syst})\,^{+0.8}_{-0.7}\,(\text{lumi})$
eμ ($\geq$ 1 jet)	$7.2^{+1.4}_{-1.3}\,(\text{stat})\,^{+0.8}_{-0.7}\,(\text{syst})\,\pm\,0.6\,(\text{lumi})$
$\mu\mu$	$5.1^{+3.4}_{-2.8}\,(\text{stat})\,^{+1.3}_{-1.1}\,(\text{syst})\,^{+0.7}_{-0.6}\,(\text{lumi})$
eτ	$8.9^{+3.3}_{-2.8}\,(\text{stat})\,^{+1.9}_{-1.8}\,(\text{syst})\,^{+0.6}_{-0.5}\,(\text{lumi})$
$\mu\tau$	$6.4^{+3.1}_{-2.7}\,(\text{stat})\,^{+2.1}_{-2.0}\,(\text{syst})\,^{+0.5}_{-0.4}\,(\text{lumi})$

and for the $\ell\ell$ and $\ell\tau$ channels combined:

$$\sigma_{t\bar{t}} = 7.5^{+1.0}_{-1.0}\,(\text{stat})\,^{+0.7}_{-0.6}\,(\text{syst})\,^{+0.6}_{-0.5}\,(\text{lumi})\,\text{pb}.$$

Both results are derived for m_t=170 GeV. These represent the most precise $t\bar{t}$ cross section measurements published so far in the dilepton channel.

To improve the statistical uncertainty in the $\ell\tau$ channels, contributions from $t\bar{t}$ events in which the τ leptons are mimicked by jets are added to the analysis. Using only $t\bar{t}$ events that decay specifically to $\ell\tau$ final states, we measure:

$$\sigma_{t\bar{t}} = 7.6^{+4.9}_{-4.3}(\text{stat})^{+3.5}_{-3.4}(\text{syst})^{+1.4}_{-0.9}(\text{lumi})\ \text{pb}$$

A measurement of the cross section multiplied by the branching ratio ($\sigma_{t\bar{t}} \times B$) has also been performed in the $\ell\tau$ channel using the acceptance from $t\bar{t}$ events that decay specifically to $\ell\tau$ final states (where only hadronically decaying τ leptons are considered). The expected contribution from other $t\bar{t}$ events is normalized using the theoretical cross section [21]. In the combined $e\tau$ and $\mu\tau$ channels we obtain the value for $\sigma_{t\bar{t}} \times B(t\bar{t} \to \ell\tau b\bar{b})$:

$$\sigma_{t\bar{t}} \times B = 0.13^{+0.09}_{-0.08}(\text{stat})^{+0.06}_{-0.06}(\text{syst})^{+0.02}_{-0.02}(\text{lumi})\ \text{pb},$$

for m_t=170 GeV, which is in good agreement with the SM expectation of 0.14 ± 0.02 pb [3, 23]. Dividing the $\sigma_{t\bar{t}} \times B(t\bar{t} \to \ell\tau b\bar{b})$ measurement by the SM expectation, we can set an upper limit on the ratio of 2.3 at 95% confidence level (CL).

The value of quark masses depends on the perturbative QCD renormalization scheme, and can differ considerably for, e.g., pole mass or $\overline{\rm MS}$ mass definitions [24]. It is therefore important to extract the mass of the top quark through a well-defined renormalization scheme. Direct top quark mass measurements compare measured distributions to distributions simulated by LO MC generators. Like any LO calculation, these MC generators are not precise enough to fix the renormalization scheme, which leads to uncertainty in the input mass definition. In the present analysis, we extract the mass of the top quark using the measured top pair production cross section. This has the advantage of not relying on simulation of the $t\bar{t}$ signal, except for determining detection efficiency. The sensitivity to any differences between the pole mass and the mass used in the MC simulation is thereby reduced relative to a direct mass measurement. We compare our result to fully inclusive $t\bar{t}$ cross sections calculated in higher-order QCD that includes soft gluon resummations, which are currently the most complete calculations available. The cross sections are computed using the pole mass definition for the top quark which is thus the parameter extracted here.

We extract the $t\bar{t}$ cross section $\sigma_{t\bar{t}}$ combining the $\ell\ell$ and $\ell\tau$ channels using the selections described above and different values of the top quark mass for calculating detection efficiencies in fully simulated $t\bar{t}$ events. The result is extracted using the same function as given in Ref. [23],

$$\sigma_{t\bar{t}} = \frac{1}{m_t^4}[a + b(m_t - 170) + c(m_t - 170)^2 + d(m_t - 170)^3]$$

with $a = 6.28727 \times 10^9, b = 9.12630 \times 10^7, c = 8.38430 \times 10^5$ and $d = -3.898 \times 10^5$ and where $\sigma_{t\bar{t}}$ and m_t are in pb and GeV respectively.

Figure 3 compares this parameterization of the combined measurement with a prediction including soft gluon resummation effects [23] and an approximate NNLO computation [25]. For the theoretical computation we plot a 68% CL interval that we determine based on Ref. [23] or [25]. The uncertainty from the ambiguity in the scale of QCD (which are varied from $m_t/2$ to $2m_t$) is represented by a likelihood function that is constant within the ranges given in Ref. [23] or [25] and vanishes elsewhere. The uncertainty due to the parton distribution functions is represented by a Gaussian likelihood, with rms equal to the uncertainty determined in Ref. [23] or [25]. For every value of the mass of the top quark, we form a joint normalized likelihood function based on the theoretical likelihoods and on a likelihood for the measurement constructed from a Gaussian with rms equal to the total experimental uncertainty [26]. We find $m_t = 171.5^{+9.9}_{-8.8}$ GeV at 68% CL using Ref. [23] and $m_t = 173.3^{+9.8}_{-8.6}$ GeV at 68% CL using Ref. [25]. These

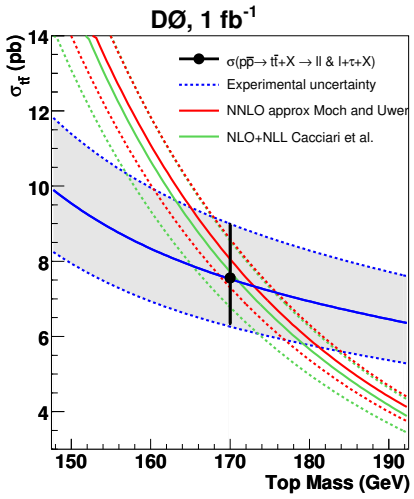

FIG. 3: Dependence of the experimental and theoretical [23, 25] $t\bar{t}$ cross section on m_t. The point shows the combination of the $\ell\ell$ and $\ell\tau$ measurements presented in this Letter.

values are in agreement with the current world average of $m_t = 172.4 \pm 1.2$ GeV [27], indicating that any deviation of the directly measured mass from the true pole mass of the mass of the top quark is $\lesssim 10$ GeV at 68% CL.

In summary, we described in this Letter the measurement of the $t\bar{t}$ cross section in the dilepton and lepton+τ channels using approximately 1 fb^{-1} of D0 data. The combined cross section is measured to be: $\sigma_{t\bar{t}} = 7.5^{+1.0}_{-1.0}\,(\text{stat})\,^{+0.7}_{-0.6}\,(\text{syst})\,^{+0.6}_{-0.5}\,(\text{lumi})$ pb for a mass of the top quark of m_t=170 GeV, in agreement with the QCD prediction. We measured $\sigma_{t\bar{t}} \times B(t\bar{t} \to \ell\tau b\bar{b}) = 0.13^{+0.09}_{-0.08}(\text{stat})^{+0.06}_{-0.06}(\text{syst})^{+0.02}_{-0.02}(\text{lumi})$ pb which agrees with the SM expectation. Using both the $t\bar{t}$ cross section measurement and the theoretical prediction, we extract the mass of the top quark: $m_t = 173.3^{+9.8}_{-8.6}$ GeV which is consistent with the mass of the top quark from direct measurements.

We thank the staffs at Fermilab and collaborating institutions, and acknowledge support from the DOE and NSF (USA); CEA and CNRS/IN2P3 (France); FASI, Rosatom and RFBR (Russia); CNPq, FAPERJ, FAPESP and FUNDUNESP (Brazil); DAE and DST (India); Colciencias (Colombia); CONACyT (Mexico); KRF and KOSEF (Korea); CONICET and UBACyT (Argentina); FOM (The Netherlands); STFC (United Kingdom); MSMT and GACR (Czech Republic); CRC Program, CFI, NSERC and WestGrid Project (Canada); BMBF and DFG (Germany); SFI (Ireland); The Swedish Research Council (Sweden); CAS and CNSF (China); and the Alexander von Humboldt Foundation (Germany).

[a] Visitor from Augustana College, Sioux Falls, SD, USA.
[b] Visitor from Rutgers University, Piscataway, NJ, USA.
[c] Visitor from The University of Liverpool, Liverpool, UK.
[d] Visitor from II. Physikalisches Institut, Georg-August-University, Göttingen, Germany.
[e] Visitor from Centro de Investigacion en Computacion - IPN, Mexico City, Mexico.
[f] Visitor from ECFM, Universidad Autonoma de Sinaloa, Culiacán, Mexico.
[g] Visitor from Helsinki Institute of Physics, Helsinki, Finland.
[h] Visitor from Universität Bern, Bern, Switzerland.
[i] Visitor from Universität Zürich, Zürich, Switzerland.
[‡] Deceased.

[1] CDF Collaboration, F. Abe et al., Phys. Rev. Lett. **74** (1995) 2626.
[2] D0 Collaboration, S. Abachi et al., Phys. Rev. Lett. **74** (1995) 2632.
[3] Particle Data Group, C. Amsler et al., Phys. Lett. B **667** (2008) 1.
[4] See, for instance, P. Fayet, S. Ferrara, Phys. Rep. **32** (1977) 249; H.P. Nilles, Phys. Rep. **110** (1984) 1.
[5] D0 Collaboration, V.M. Abazov et al., Phys. Rev. D **76** (2007) 052006.
[6] CDF Collaboration, D. Acosta et al., Phys. Rev. Lett. **93** (2004) 142001.
[7] D0 Collaboration, V.M. Abazov et al., Nucl. Instrum. Methods Phys. Res. Sect. A **565** (2006) 463.
[8] The pseudorapidity is defined as $\eta = -\ln[\tan(\theta/2)]$ where θ is the polar angle with respect to the proton beam.
[9] D0 Collaboration, S. Abachi et al., Nucl. Instrum. Methods Phys. Res. Sect. A **338** (1994) 185.
[10] D0 Collaboration, V.M. Abazov et al., Nucl. Instrum. Methods Phys. Res. Sect. A **552** (2005) 372.
[11] C.F. Galea, Acta Phys. Pol. B **38** (2007) 769.
[12] G.C. Blazey et al., arXiv:hep-ex/0005012 (2000).
[13] T. Scanlon, Ph.D. thesis, Imperial College, University of London (2006), FERMILAB-THESIS-2006-43.
[14] M.L. Mangano et al., JHEP **0307** (2003) 001, ALPGEN version 2.05.
[15] T. Sjöstrand et al., Comp. Phys. Commun. **135** (2001) 238, PYTHIA version 6.319.
[16] R. Brun, F. Carminati, CERN Program Library Long Writeup W5013, 1993 (unpublished).
[17] J.M. Campbell, R.K. Ellis, Phys. Rev. D **60** (1999) 113006.
[18] J.M. Campbell, R.K. Ellis, MCFM - Monte Carlo for FeMtobarn processes, http://mcfm.fnal.gov; R.K. Ellis, Nucl. Phys. Proc. Suppl. **160** (2006) 170.
[19] J. Smith, W.L. van Neerven, J.A.M. Vermaseren, Phys. Rev. Lett. **50** (1983) 1738.
[20] T. Andeen et al., FERMILAB-TM-2365 (2007).
[21] N. Kidonakis, R. Vogt, Phys. Rev. D **78** (2008) 074005.
[22] P. Sinervo, in *Proceedings of Statistical methods in Particle Physics, Astrophysics, and Cosmology*, edited by L. Lyons, R. Mount, R. Reitmeyer (SLAC, Standford, 2003), p334.
[23] M. Cacciari et al., JHEP **09** (2008) 127; M. Cacciari, private communications.
[24] N. Gray et al., Z. Phys. C **48** (1990) 673; K. Melnikov, T. v. Ritbergen, Phys. Lett. B **482** (2000) 99; K.G. Chetyrkin, M. Steinhauser, Phys. Rev. Lett. **83** (1999) 4001.
[25] S. Moch, P. Uwer, Phys. Rev. D **78** (2008) 034003.
[26] D0 Collaboration, V.M. Abazov et al., Phys. Rev. Lett. **100** (2008) 192004.
[27] The Tevatron Electroweak Working Group for the CDF and D0 Collaborations, *A combination of CDF and D0 results on the mass of the top quark*, arXiv:0808.1089 [hep-ex] (2008).